Journal of Sol-Gel Science and Technology (2023) 108:655–671
https://doi.org/10.1007/s10971-023-06210-x

ORIGINAL PAPER: SOL-GEL AND HYBRID MATERIALS FOR BIOLOGICAL AND HEALTH (MEDICAL) APPLICATIONS

Solar energy driven photo catalytic action and antimicrobial activities of Iron oxide nanoparticles

Tanzeela Batool[1] · Zaheer H. Shah[1,2] · Hina Ashraf[1,3] · Daoud Ali[4] · S. Shamaila[5] · Tehmina Anjum[3] · Shahzad Naseem[1] · Saira Riaz[1]

Received: 11 October 2022 / Accepted: 8 August 2023 / Published online: 5 September 2023

Abstract

Every year loss of crop yield (at least 20–40%) occurs by pathogenic infections that leads to loss of billions of dollars worldwide. Usage of antibiotics are limited in numerous countries for controlling bacterial diseases / infections in agricultural field. Therefore, alternative protocol is necessary to combat with microbial pathogens and to overcome the requirement to suppress use of conventional antibiotics in plant production. Nanoparticles (NPs) having antimicrobial properties can have potential to combat the bacteria and can protect the plant / crop production. Moreover, such NPs may also have potential to suppress the plant pathogens. Sol-gel method is used for synthesis of iron oxide NPs with variation in pH (1, 2, 3, 4, 5, 6, 7, 8 and 9). Magnetic field annealing (MFA) of NPs at different temperatures (200 and 300 °C) is done. 300 °C MFA samples show efficient results. X-ray Diffraction (XRD) results show magnetite phase (at pH 1, 2 and 6), mixed phases (i.e. hematite and maghemite) at pH 3–5, maghemite phase (at pH 7-8) and hematite phase (at pH 9) of iron oxide. Scanning Electron Microscopy (SEM) analysis shows particle size of ~50 nm for MFA iron oxide NPs (at pH 6). Raman spectroscopy results show the formation of iron oxide NPs. Furthermore, 300 °C MFA magnetite nanoparticles (at pH 6) proved to be potential candidate against bacteria (*E. coli* with inhibition zone ~31 mm) and against methylene blue with enhanced photo catalytic action. In-vitro activity of magnetite NPs expressively inhibited the growth of Fusarium oxysporum after 3rd and 7th day of incubation in a dose-dependent way. In-vivo studies also exhibited improved plant growth parameters after treatment with different concentrations of magnetite NPs. This work suggests that iron oxide NPs can be used in agricultural sector for protection of plant.

Graphical Abstract

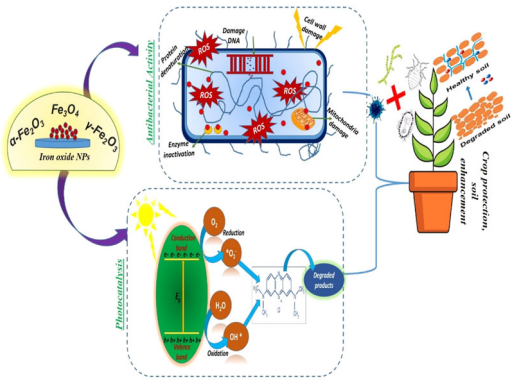

✉ Saira Riaz
saira.cssp@pu.edu.pk

[1] Centre of Excellence in Solid State Physics, University of the Punjab, Lahore 54590, Pakistan

[2] Department of Physics, University of Management and Technology, Lahore, Pakistan

[3] Department of Plant Pathology, University of the Punjab, Lahore 54590, Pakistan

[4] Department of Zoology, College of Science, King Saud University, Riyadh 11451, Saudi Arabia

[5] Waterloo institute for Nanotechnology, University of Waterloo, Waterloo, ON, Canada

Keywords Iron oxide · Photocatalytic · Antibacterial · Crop · Protection

Highlights

- Sol–gel method was employed for synthesis of iron oxide NPs by varying pH values (1–9).
- Magnetite phase was observed for pH 1, 2 and 6.
- Particle size of ~50 nm was observed for magnetite NPs.
- Magnetite NPs (pH 6) showed remarkable antifungal activity during in vitro and in vivo tests.
- Magnetite NPs can be suitable for protection of crops and degradation of dyes/organic pollutants.

1 Introduction

Iron oxide nanoparticles (NPs) have got worldwide attention due to their high surface to volume ratio along with outstanding structural, optical, magnetic, antimicrobial and electrical properties that make it an exceptional choice to be used in photo catalytic and antibacterial applications [1–3]. Biocompatibility of iron oxide NPs depends upon two parameters i.e. size of magnetic NPs and magnetic interactions of moments [4]. The magnetic properties of such NPs can be controlled from superparamagnetic to ferromagnetic with variation in size and pH value [5]. NPs having small size have greater penetration and possibility for cell destruction against bacterial membrane [6]. Moreover, iron oxide NPs having appropriate bandgap can resist in oxidative environments efficiently and are thus suitable candidate for photocatalytic activity [7].

Well known stable phases of iron oxide are hematite (α-Fe_2O_3), maghemite (γ-Fe_2O_3) and magnetite (Fe_3O_4) [8]. Both magnetite and maghemite exhibit inverse spinel cubic structure with ~ 850 K and ~ 863–945 K Neel's temperature (T_N), respectively [9]. Magnetite has inverse spinel crystal structure with face-centered cubic unit cell. In crystal structure of magnetite, ferrous ions (i.e. Fe^{2+}) and half of the ferric ions (i.e. Fe^{3+}) take place on octahedral sites and other half of Fe^{3+} takes place on tetrahedral sites. In contrast, hematite phase is tightly packed in a configuration that includes Fe^{3+} ions in octahedral coordination with oxygen atoms [10].

Physical properties of nanoparticles with various phases along with optimization according to the application depends upon structure, morphology and synthesis method of NPs. For preparation of iron oxide NPs, hydrothermal [11], co-precipitation [12–14], thermal decomposition [15], sol-gel [16], pulsed laser ablation [6], sequential one-pot method [17] and thermal evaporation [18] proved to be effective for antibacterial and photo catalytic activity. However, in all of the synthesis methods pre / post treatments with usually high temperatures are utilized along with usage of complex reagents. In the present work, sol-gel method is used for preparation of iron oxide NPs due to its merits over other methods. In this method, colloidal suspension is attained by hydroxylation and condensation of precursors. It is also low cost with time saving method. This technique has good control not only in synthesis process but also on gaining stable phases without use of high temperatures which leads to homogeneous desired systems [19–23].

Nanoparticles, with their remarkable antibacterial effects, can have their applications in agriculture field to decrease waste generation, increase crop yield and to protect water when compared with common pesticides. Such NPs can disturb cell wall, cytoplasmic membrane, energy and electron transfer chain, protein / DNA (Deoxyribonucleic acid) oxidation and inhibition of enzymes that enhances their use in pesticides and fungicides [24–26]. Generally, inorganic materials are found to be stable and have outstanding antibacterial properties as compared to organic ones [27]. Iron oxide NPs have important role in antibacterial applications, but still biocompatible materials are more favorable that can functionalize the surface of NPs to enhance their properties and have fewer toxic effects to healthy tissues. Many researchers functionalized iron oxide NPs to improve different properties along with controlling their instability [28, 29]. Functionalization helps in controlling aggregation and stability of small sized NPs [30]. Thus, various polymers and oligomers can be designed/synthesized for specific applications. Polyethylene glycol has been used to modify the surface morphology of metal oxides. Ethylene glycol, when used as solvent, shows uniform surface morphology along with low dielectric losses. These properties have been observed because of the latent heat of vaporization along with molecular structure of ethylene glycol [31–34]. Nisin-loaded iron oxide nanoparticles demonstrated antimicrobial response [35].

Annealing has vital role in boosting physical properties of metal oxide nanoparticles. Further, annealing process can change amorphous nature and agglomeration of NPs into crystalline nature [36]. Transition in phases and magnetism are reported in different projects with effect of thermal annealing for iron oxide NPs [37, 38]. Annealing, under the external magnetic field, is performed and termed as magnetic field annealing (MFA). Reorientation of easy axis occurs in magnetic material as a result of MFA. Importance of MFA lies in enhancement of magnetic structures by eliminating defects [39]. Prabhu et al. [40] reported antibacterial

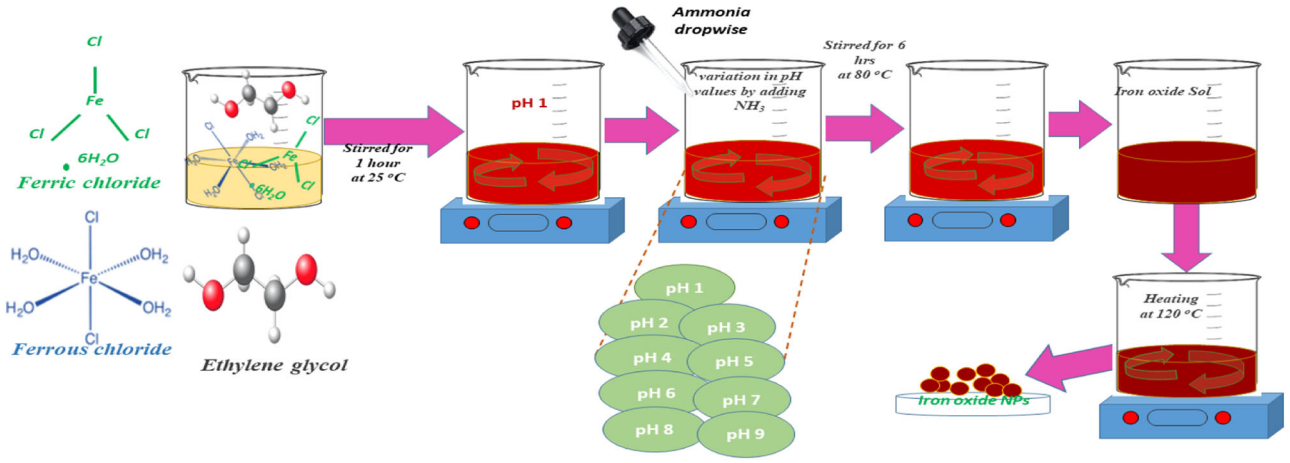

Fig. 1 Schematic for synthesis of Iron oxide NPs

performance of magnetite NPs with different concentrations ((25, 30–60 (with interval of 10), 80, 100) µg/ml) of NPs. Potential antibacterial activity was attained at higher concentrations of Fe_3O_4 NPs against *E.coli* strains i.e. 21 mm zone of inhibition. Herrera et al. [41] prepared iron oxide-TiO_2 nanomaterials and checked their photocatalytic activity. XRD patterns showed the cubic inverse spinel structure of iron oxide NPs (maghemite / magnetite) and anatase phase of TiO_2 NPs. Crystallite size of iron oxide NPs and TiO_2 was found to be ~30 and ~19 nm, respectively. Photo degradation activity under Ultraviolet irradiation in chamber for 6 h was done using different concentrations of nanocomposite. Maximum 89 % of phenol photo degradation was achieved.

Nanoparticles with photo-catalytic action are being studied for toxic compounds' degradation. However, literature on suppressing microbial pathogens along with photo catalytic materials are less available. To authors' best knowledge, synthesis of iron oxide nanoparticles without any acids as stabilizer are not yet investigated for enhanced solar light driven photo catalytic along with antimicrobial activities. Sol-gel synthesized iron oxide nanoparticles are expected to show an excellent degradation activity in the degradation of methylene blue and killing of *Escherichia coli (E. coli)* bacteria. Iron oxide NPs have potentially controlled the fungal growth by improving plant growth parameters. In the selection of bacteria, *E. coli* was chosen due to its usual occurrence in contaminated water.

2 Experimental details

2.1 Materials

Iron (II) chloride tetrahydrate [$FeCl_2.4H_2O$], iron (III) chloride hexahydrate [$FeCl_3.6H_2O$], ethylene glycol ($C_2H_6O_2$) and ammonia (NH_3) were obtained from Sigma-Aldrich. Ferrous and Ferric chloride were used as starters whereas ethylene glycol was used as a solvent. Moreover, pH of sols was varied using NH_3.

2.1.1 Synthesis method

Sol-gel method was used to obtain iron oxide nanoparticles. Ferric chloride (1.35 g) and ferrous chloride (0.99 g) were dissolved in ethylene glycol (50 ml). This solution was stirred at room temperature (25 °C) for 1 hr to get transparent sol (reddish brown) with pH 1. pH of sols was varied (1–9) with interval of 1 using ammonia. Then sols were heated at 80 °C on hot plate for 6 h. Further, heating at 120 °C leads to production of iron oxide NPs. Schematic diagram for preparation of iron oxide nanoparticles is depicted in Fig. 1. After that magnetic field annealing (MFA) at 200 and 300 °C for 1 hr was done.

2.2 Antibacterial activity

Antibacterial performance of magnetic field annealed iron oxide NPs was performed against *Escherichia coli (E. coli)* bacterial strain. Autoclaved petri plates were filled with 20 ml of Muller-Hinton agar (MHA) and then let MHA to be solidified. Bacteria was streaked evenly onto MHA. Wells were made and different dilutions of iron oxide NPs were dispensed into wells. Then, all plates were placed for incubation at 37 °C for 24 h. Afterwards, zone of inhibition, using ruler (in mm units), was measured.

2.3 Photo catalytic activity

The photo catalytic activity was studied by photo degradation of methylene blue (MB) solution under direct sunlight in the month of June 2022. Photo catalytic activity was

performed using appropriate amount of catalyst in airtight bottles containing methylene blue (5.0 ml). Before exposing to solar radiation, all bottles were stirred in dark for 30 min to establish adsorption–desorption equilibrium between photocatalyst and dye. Samples were irradiated for 1 hr with time interval of 15 min. Percentage of MB degradation using nanoparticles was calculated from Eq. 1 [42]:

$$\text{Percentage of degradation}\,(\%) = \frac{(A_O - A)}{A_o} \times 100 \qquad (1)$$

A_o is initial absorption of MB and A is absorption after interval of time (total 60 min with interval of 15 min).

2.4 Antifungal activity

The in-vitro antifungal activity was performed using Potato Dextrose Agar (PDA). Various concentrations of iron oxide NPs (0.01, 0.05, 1.5, 2.5, 5, 7.5, 10, 12.5, 15 and 17.5 µg/ml) were prepared. A disk of fungus (5 mm) was placed in center of each plate having PDA. Plates were incubated for 7 days at 28 °C to examine the fungal growth inhibition. All trials were executed in triplicate. The inhibition growth of fungus was calculated using Eq. 2 [43].

$$\textbf{Inhibiton of radial growth}(\%) = \frac{(r1 - r2)}{r1} \times 100 \qquad (2)$$

Where r1 and r2 are radial growth of mycelium in control and treatment (nanoparticles), respectively.

3 Characterization techniques

Structural analyses were studied using X-ray diffractometer with Cukα = 1.5405 Å. Morphology was examined using Scanning electron microscope. Magnetic and optical properties were checked using Vibrating sample magnetometer (LakeShore, Series 7400 model 7407) and JA Woollam M-2000 variable angle spectrometric ellipsometer, respectively. Absorbance of photo catalytic activity was studied using Shimadzu UV-Visible spectrophotometer (UV-1800). Agar well diffusion method was adapted to perform antibacterial activity. Antifungal activity was evaluated using Potato Dextrose Agar against Fusarium oxysporum.

4 Results and discussion

4.1 XRD analysis

Fig. 2a shows XRD patterns of optimized magnetic field annealed (MFA) samples at 300 °C under all pH levels (1–9). Presence of peaks corresponding to (311), (400), (422), (511), (440), and (620) planes show the formation of magnetite phase according to card no. 001–1111 at pH 1-2 and 6 under as-synthesized condition. However, strengthening of magnetite phase of iron oxide is observed after magnetic field annealing of samples at 200 and 300 °C. This enhancement in crystalline structure, due to effect of annealing, is in accordance with literature [44]. Mixed phases (i.e. hematite and maghemite) were observed at pH 3, 4 and 5. Planes (211), (104), (110), (113), (024), (116), (018), (300) and (223) show hematite phase (α-Fe_2O_3) of iron oxide. Planes (210), (310), (311), (400), (410), (421), (422), (440) and (530), matched to maghemite (card no. 39-1346). Maghemite phase of iron oxide was observed with the increase in pH to 7-8. Further increase in pH value to 9 led to the formation of maghemite phase for as-synthesized and 200 °C MF annealed samples. Whereas, structural transformation, i.e. maghemite to hematite (γ-Fe_2O_3 to α-Fe_2O_3), was observed at 300 °C MF annealed samples. It is important to mention here that formation of various iron oxide phases may address variety of technological applications including electronics, spintronics, biological and catalysis [45].

Crystallite size (D) and dislocation density (δ) were calculated for as-synthesized and annealed samples using Eq. 3-4 respectively [46].

$$D = \frac{k\lambda}{\beta \cos\theta} \qquad (3)$$

$$\text{Dislocation density} = \frac{1}{D^2} \qquad (4)$$

Where, k is shape factor (0.9), λ is wavelength and β is full width at half maximum. Variation in values of D and δ with pH is shown in Fig. S1(a-b). However, crystallite size and dislocations of samples annealed at 300 °C are shown here (Fig. 2b). Results illustrated enhanced impact of MFA on crystallite size. It facilitates the growth of different grain sizes and thus increase in crystallite size can be seen for all samples of iron oxide NPs. MFA helps in overcoming different energies of each grain and tends to increase crystallite size of iron oxide NPs [47]. The strengthening of already existing phases with MFA is in accordance with literature [39, 44]. Acidic and alkaline nature of solution in chemical reaction slows down and facilitates hydrolysis process, respectively [48]. Fig. 2b shows the presence of four different regions in the values of crystallite size and dislocation density. These regions agreed well with the appearance of various iron oxide phases under different synthesis conditions, i.e. variation in pH value, as discussed for Fig. 2a. Solutions' acidic nature is responsible for decreased crystallite size at low pH levels of as-synthesized samples [Fig. S1(a)]. Whereas MF annealing led to increased crystallite size along with phase strengthening. As discussed earlier, hydrolysis rates get fast in alkaline

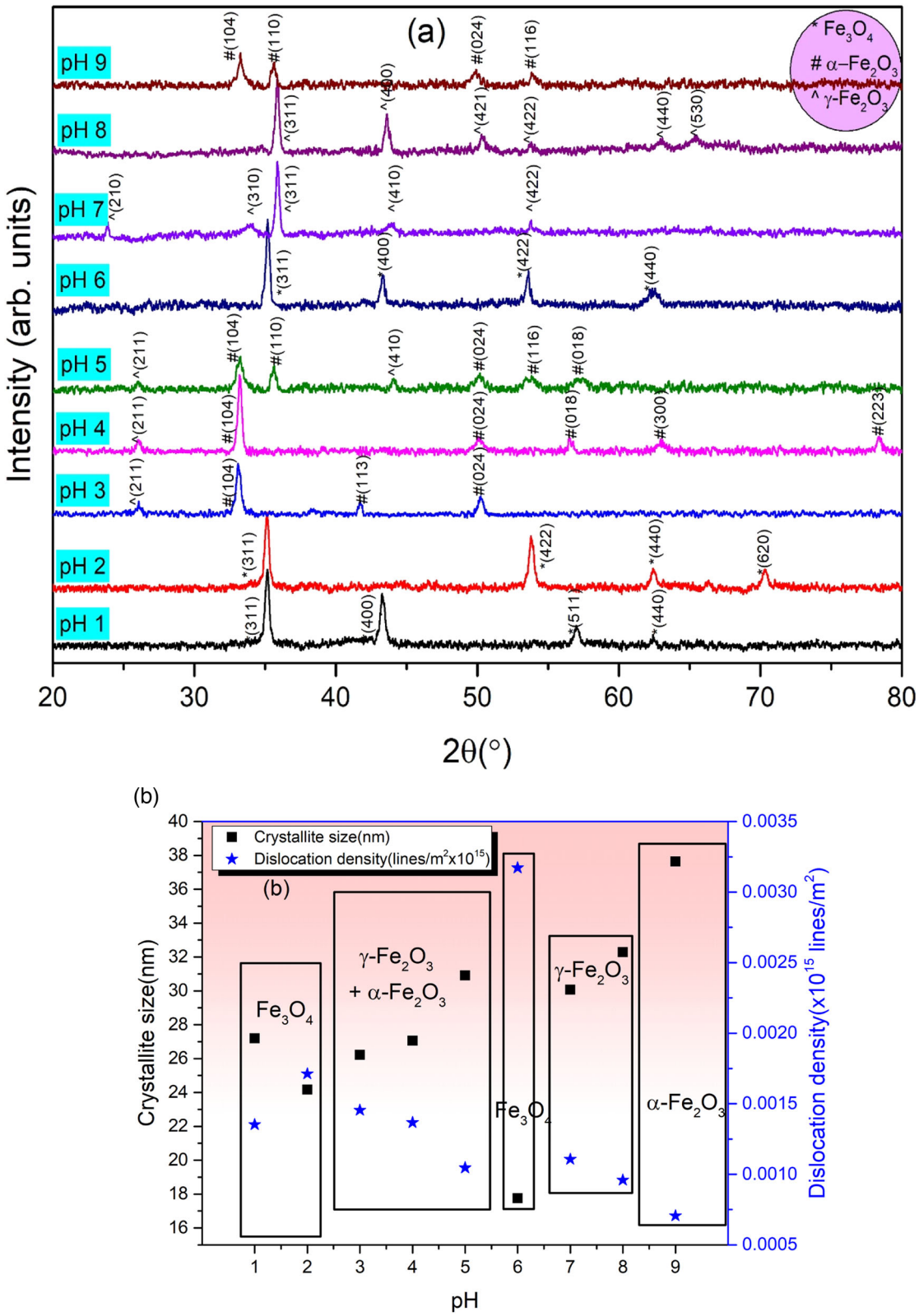

Fig. 2 **a** XRD pattern and **b** crystallite size for MFA sample at 300 °C iron oxide NPs at pH (1–9)

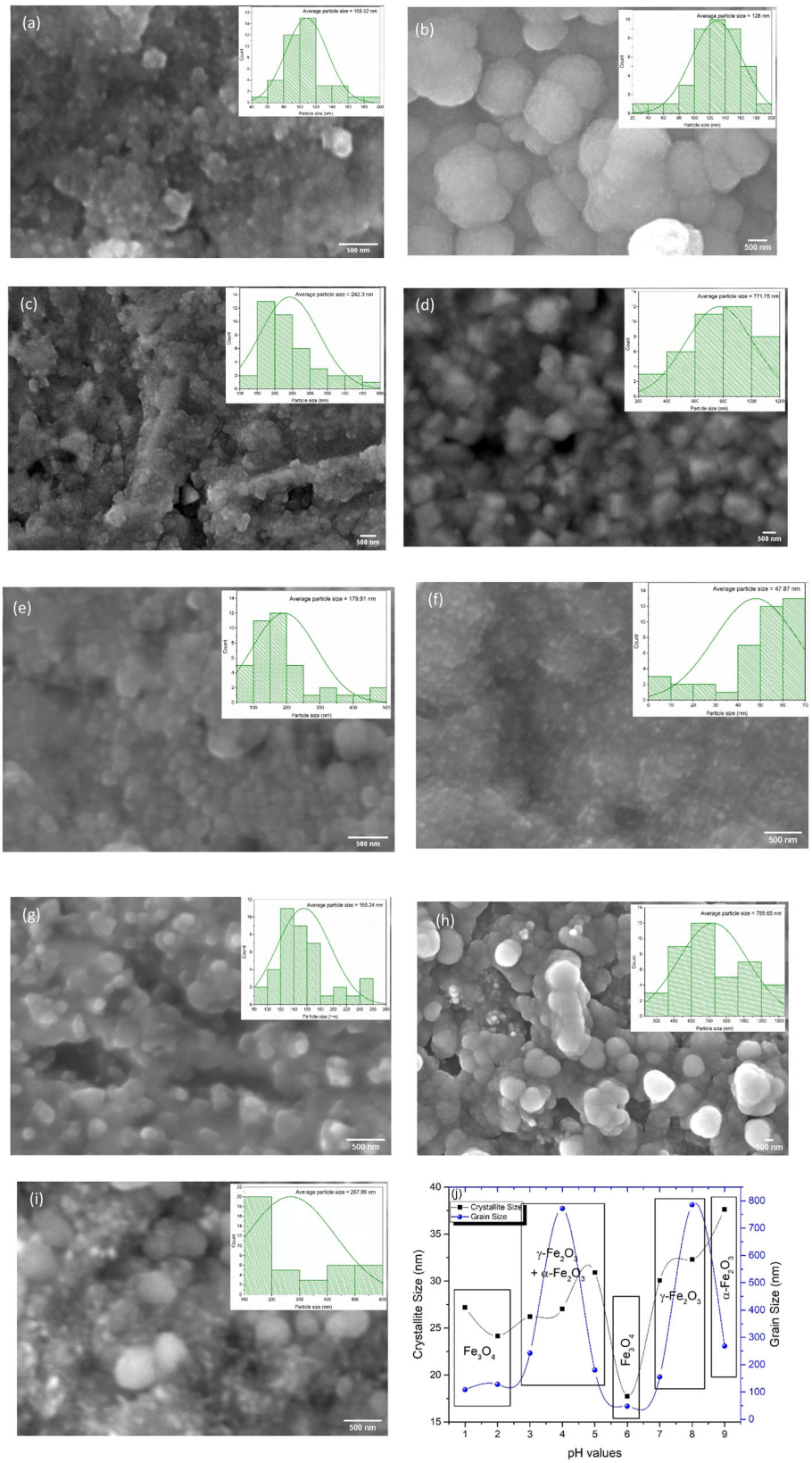

Fig. 3 SEM images of iron oxide NPs prepared with pH (**a**) 1, (**b**) 2, (**c**) 3, (**d**) 4, (**e**) 5, (**f**) 6, (**g**) 7, (**h**) 8 and (**i**) 9 and (**j**) relation of crystallite and grain size

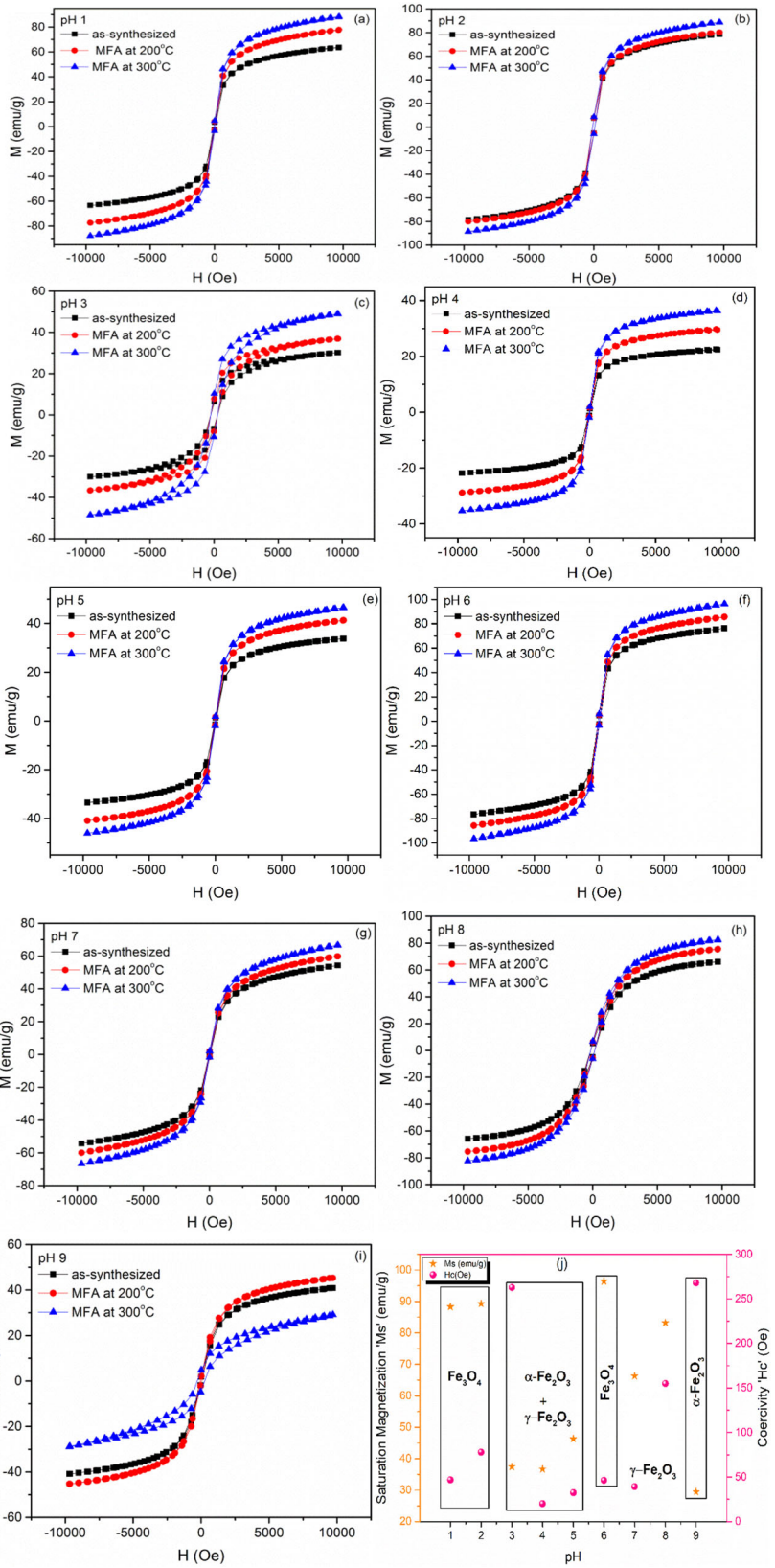

Fig. 4 **a–i** M-H curves and (**j**) variation of M_s and H_c as a function of pH for 300 °C MFA iron oxide NPs

environment (pH greater than 6) resulting in increased crystallite size for all prepared samples. Polymerization of colloidal particles occurs in sol-gel method leading to increased crystallite size with increasing pH values. Presence of ethylene glycol during synthesis may lead to slow aggregation that helps in adequate rotation / movement of nanocrystallites that give stress-free NPs [49]. In the current study, chemical shifts / phase transformation and restructuring are responsible for increase or decrease of dislocation density and crystallite size, respectively and is in agreement with literature [50].

4.2 SEM analysis

SEM images of magnetic field annealed samples (at 300 °C) synthesized at various pH values are shown in Fig. 3. Variation in sols' pH gives variation in particle sizes. Small-sized particles possess reaction dynamics due to high surface energy generation, whereas large-sized particles are thermodynamically preferred due to large bulk energy. Hence, particle size can be controlled by varying pH for different phases. The microscopic images of iron oxide NPs with pH varying levels (1, 2 and 6) showed soft agglomeration of spherical particles with diameter of ~50 nm at pH 6. Whereas particles with relatively hard agglomeration and increased size were observed for pH 4-5. Spherical particles with large diameter were observed at higher pH values of 7–9. Particle size observed under various pH conditions has been correlated with the crystallite size obtained using XRD data (Fig. 3j).

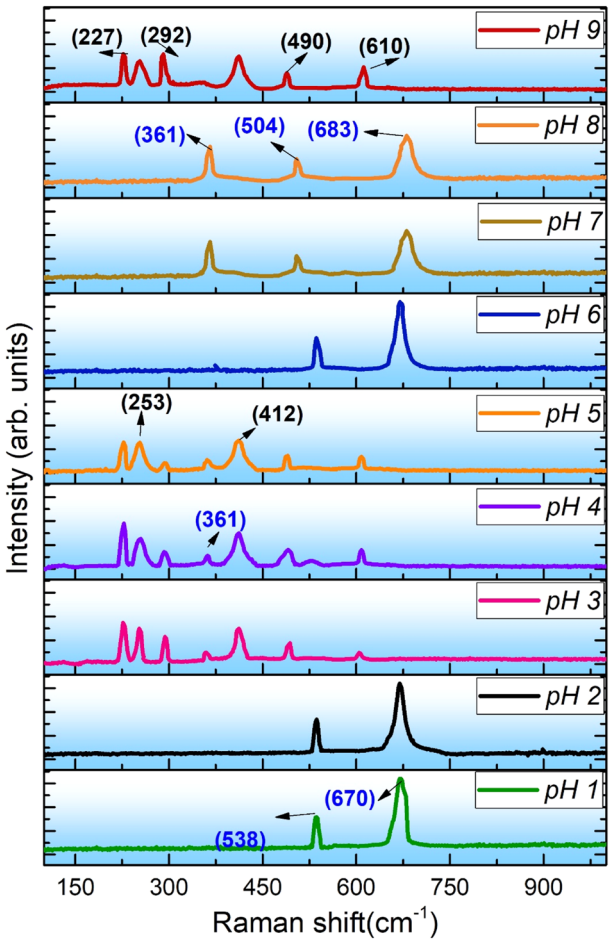

Fig. 5 Raman analysis of iron oxide NPs with pH variation (1–9)

4.3 Magnetic analysis

M-H curves for iron oxide NPs at room temperature are shown in Fig. 4. Crystallite size, specific phase, surface morphology and distribution of cations are strongly responsible for magnetic properties [51]. Samples prepared with pH 1, 2, 6 and 9 exhibited superparamagnetic nature with high value of saturation magnetization (M_s) for nanoparticles prepared with pH 6. Ferromagnetic behaviour was observed for pH 3–5 and 7-8. Superparamagnetic nature with high value of M_s can be associated with small particle size of iron oxide NPs. All these findings are consistent with XRD and SEM results discussed for Figs. 2–3. Variation in saturation magnetization (M_s) of iron oxide NPs for all pH levels (1–9) is shown in Fig. 4j. Variation in M_s can be correlated with structural results (Fig. 2a) due to size dependence of magnetic properties of NPs as discussed earlier. Significant increase in M_s values is observed after magnetic field annealing at each pH level as compared to as-synthesized samples.

MF annealing helps in alignment of domains present in material, thus, giving higher values as compared to as-synthesized samples. Multiple domains are absent in superparamagnetic NPs, so they act as an isolated magnetic domain in the system and thus exhibited high saturation magnetization. 300 °C MF annealed samples prepared with pH 1, 2 and 6 showed high values of M_s in contrast to other pH levels. Saturation magnetization values of magnetite phase of iron oxide NPs are 88.4 emu/g (at pH 1), 88.6 emu/g (at pH 2) and 96.4 emu/g (at pH 6). These obtained values are close to value of M_s (bulk) of magnetite i.e. 92 emu/g [52]. At pH 3–5 (mixed phases), M_s values are found to be 37.45 emu/g, 36.71 emu/g and 46.34 emu/g, respectively, for 300 °C MFA samples. Saturation magnetization (M_s) of 66.30 emu/g and 83.22 emu/g was observed for pH 7 and 8 (maghemite phase), respectively. Slightly increased value of saturation magnetization as compared to bulk value depends upon two parameters: (1) effect of reduced surface anisotropy and (2) effect of MF annealing in samples that accelerates alignment of domains in pre-existing phases of iron oxide NPs. Transformation of NPs from superparamagnetic to weak ferromagnetic, at pH 9 (MFA at 300 °C), is observed as a

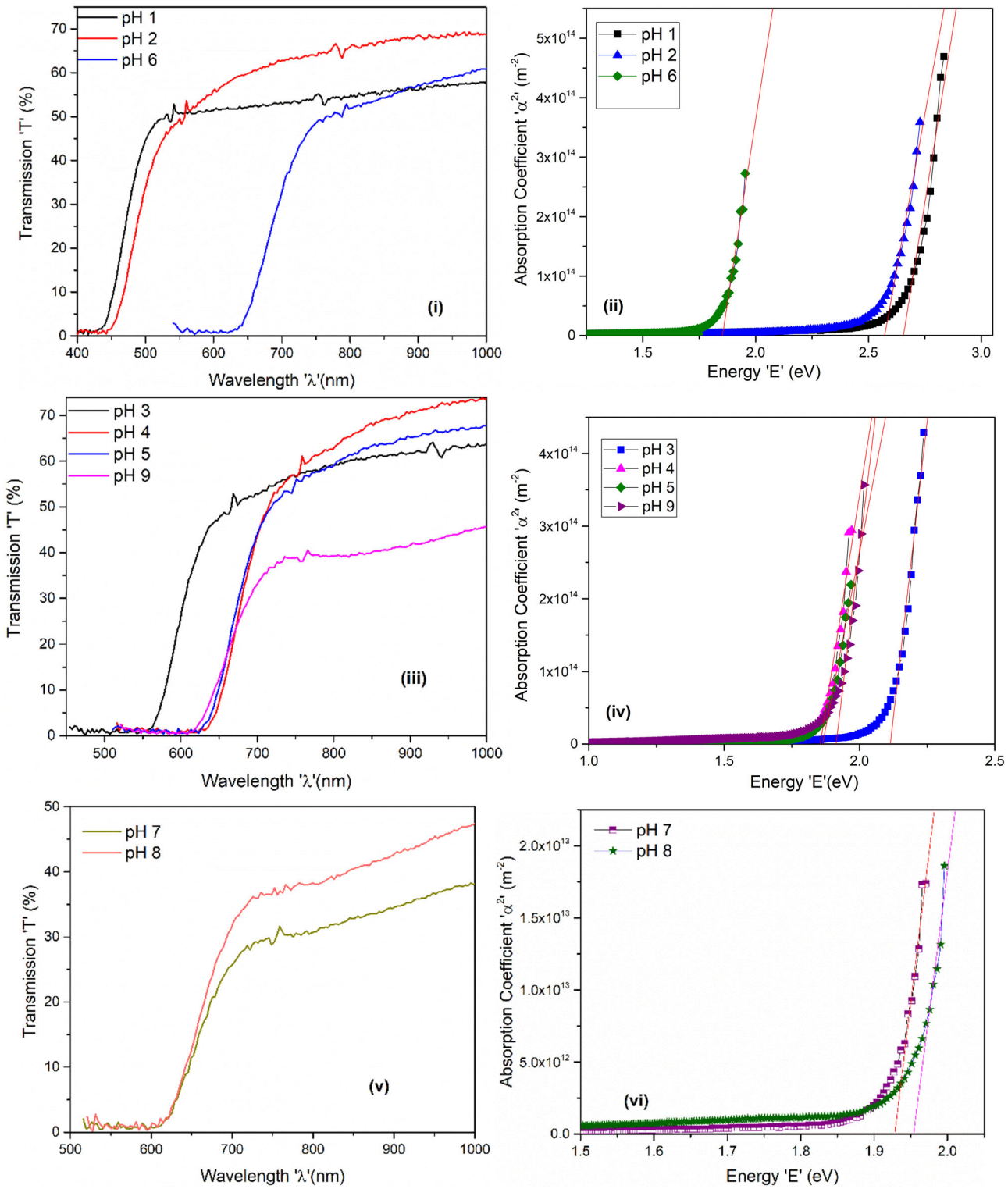

Fig. 6 Variation of transmittance (i, iii,v) and band gap (ii, iv, vi) for MFA iron oxide NPs synthesized at pH 1–9

consequence of enhanced nucleation rate as discussed earlier. Table S1 presents comparison of values of M_s for iron oxide NPs obtained from other techniques with sol-gel technique (present work).

4.4 Raman analysis

Occurrence of different phases of iron oxide NPs under different pH values were checked by Raman analyses. Fig. 5

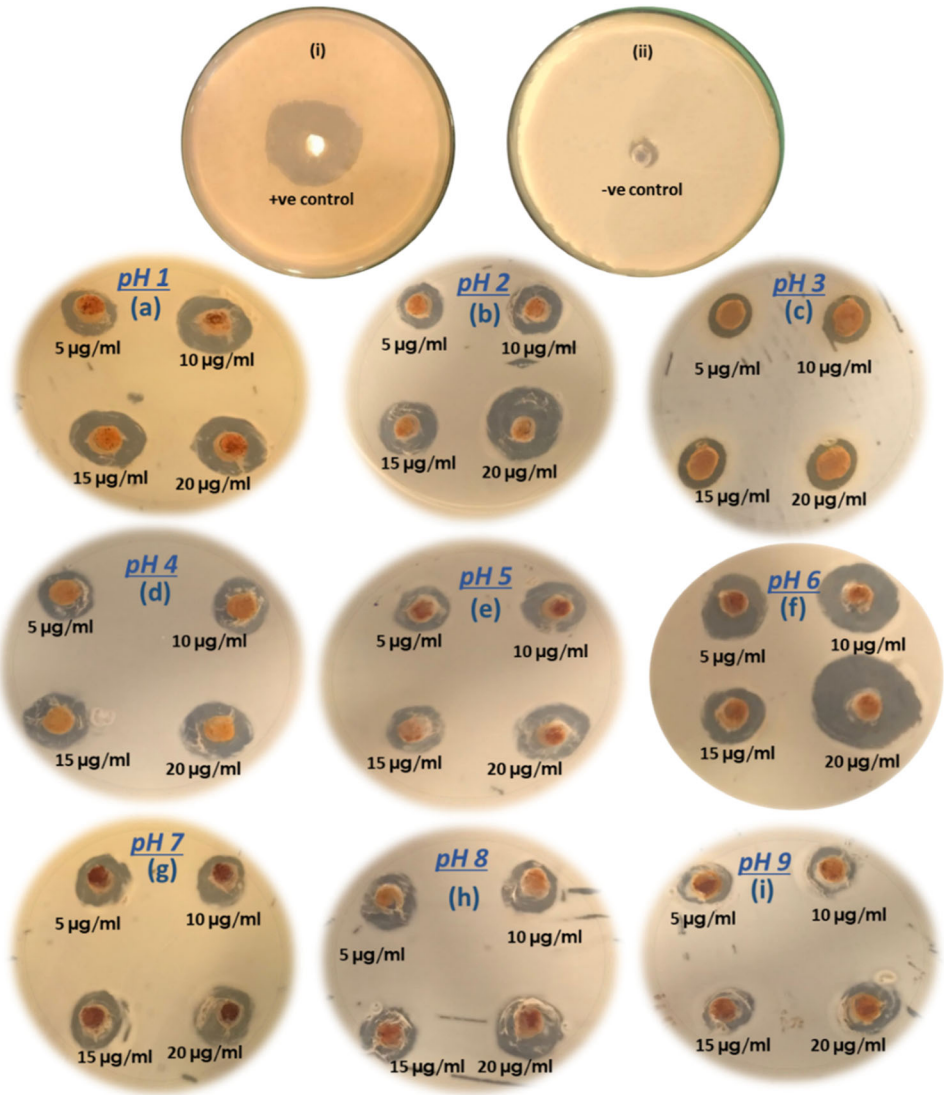

Fig. 7 (i) Positive, (ii) negative control and (**a**–**i**) antibacterial activity for iron oxide NPs against *E. coli* under pH 1–9

shows Raman spectra of iron oxide NPs for all pH levels (1–9). The specific peaks at ~ 667 cm^{-1} and ~ 525 cm^{-1} are related to A_{1g} and T_{2g} modes of iron oxide magnetite phase (Fe_3O_4) [53] and are comparable for the samples prepared with pH 1-2 and 6. The peaks around 227 and 490 cm^{-1} are associated with A_{1g} phonon mode whereas peaks around 225, 292, 406 and 600 cm^{-1} are related to E_g phonon modes for iron oxide NPs at pH 3–5 and 9. These results indicate the formation of hematite phase (α-Fe_2O_3) [54]. Three Raman active phonon modes at ~ 359, ~ 499, and ~ 677 cm^{-1} are related to T_{2g}, E_g and A_{1g}, respectively for iron oxide NPs (pH 7-8). These modes show the presence of maghemite phase (γ-Fe_2O_3) [55].

4.5 Optical analysis

Optical properties of 300 °C MF annealed (MFA) samples for all pH levels (1–9) are shown in Fig. 6(i, iii, v). Maximum transmission ~ 70 % is observed for MFA iron oxide NPs at pH 2. At pH 6 maximum transmission observed is ~ 62 %. Decrease in transmission at pH 7-8 with small shift of transmission maxima towards higher wavelength is observed. This shift might have been observed because of the phase transformation from magnetite (pH 6) to maghemite. In case of maghemite, vacant positions at tetrahedral sites lead to defects and thus decreased transmission is evident with increased scattering. At pH 9, transmission has decreased value as phase transforms to hematite from maghemite for 300 °C MFA iron oxide NPs.

Absorption coefficient was calculated for 300 °C MFA iron oxide NPs using Eq. 5 [56].

$$\alpha = \frac{1}{t} \ln\left[\frac{2R^2T}{\left\{-1(1-R)^2+\sqrt{(1-R)^4+4R^2T^2}\right\}}\right] \quad (5)$$

Where, R is reflection, T is transmission and t is thickness of nanoparticles. Graphs for band gap of 300 °C MFA iron oxide

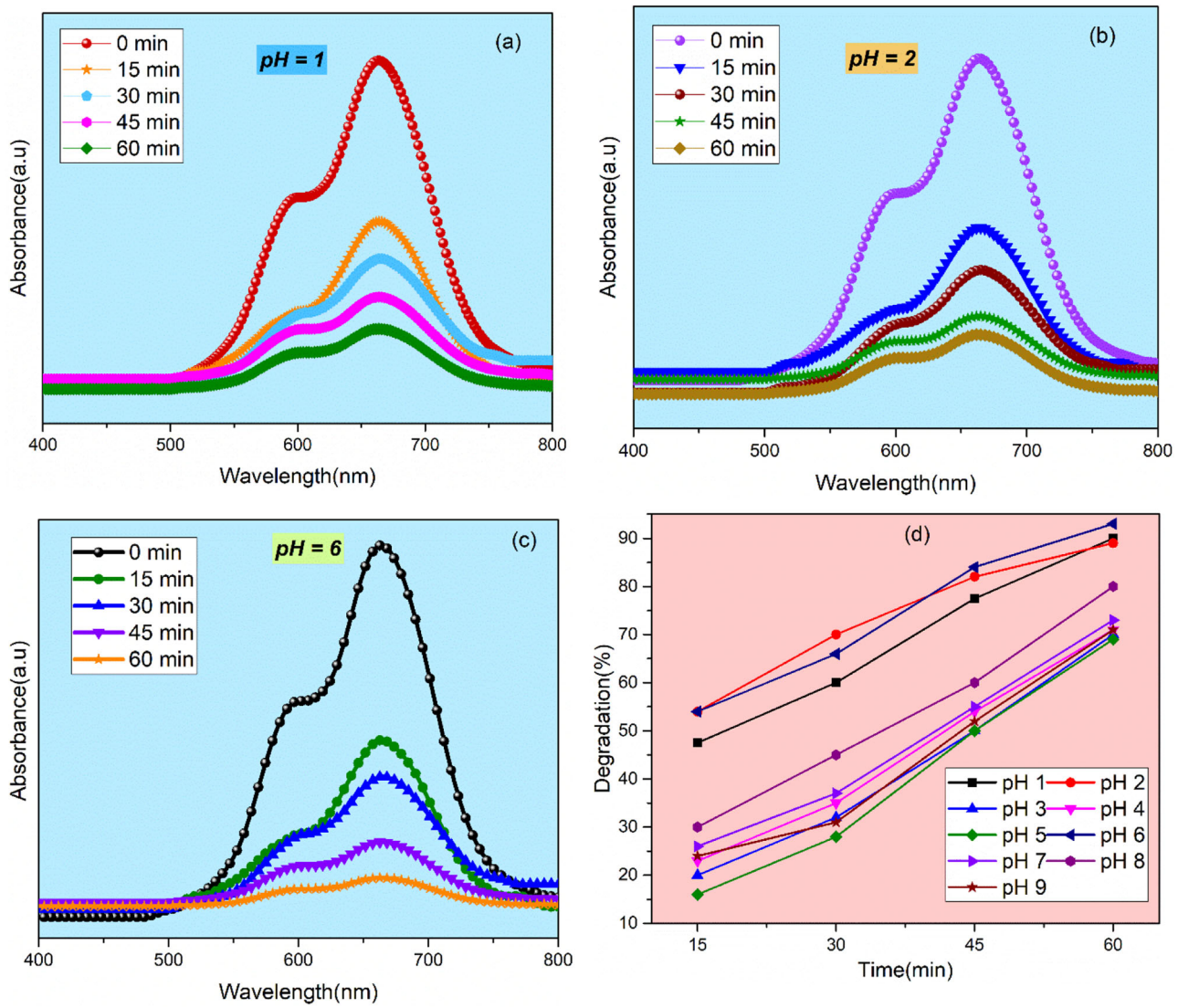

Fig. 8 **a** Photo catalytic action with variation in irradiation time at (**a**) pH 1, (**b**) pH 2, (**c**) pH 6 and (**d**) Degradation (%) of 300 °C MFA iron oxide NPs at pH 1–9

NPs are shown in Fig. 6. Direct band gap of iron oxide NPs is evaluated by extrapolating linear regions. It is obvious from results that structural and magnetic transition along with bandgap variation occurs with varying pH level. For pH 1, 2 and 6 calculated band gap is in the range of 2.6–1.85 eV. For mixed phases (pH 3–5), band gap values are in the range of 2.11–1.85 eV, for pure maghemite phase (pH 7-8), band gap values are 1.92–1.95 eV. [Fig. 6(vi)]. In case of hematite phase (pH 9), band gap value is found to be 1.94 eV. Fig. S8 illustrates the bandgap reduction with crystallite size decrement. Table S2 gives comparison of current bandgap values of magnetite with previous reported work.

4.6 Antibacterial activity

One of the serious concerns with food safety is transfer of pathogens (i.e. bacteria) from filthy soil to edible portion of crops. Therefore, it is necessary to check antibacterial activity for protection of crops from soil contamination. *E. coli* is selected as it can stay alive in soil for more than ninety days and can resist in transporting water and nutrients to rest of the plant. Ultimately, the plant begins to droop or decline. This whole process can occur within a single day. Therefore, antibacterial activity was performed against *E. coli* bacterial strain for optimized 300 °C MFA iron oxide NPs under all pH levels (1–9) with variation in concentrations (5–20 µg/ml) with interval of 5 µg/ml of NPs. Positive and negative control are also shown in Fig. 7(i-ii). Enhanced zone of inhibition is observed for all concentrations at all pH values (Fig. 7). Magnetite phase with superparamagnetic behavior synthesized at pH 6 (300 °C MFA iron oxide NPs) was found to be proficient against bacteria with ~ 31 mm zone of inhibition at highest concentration. Moreover, rest of the values of zone of

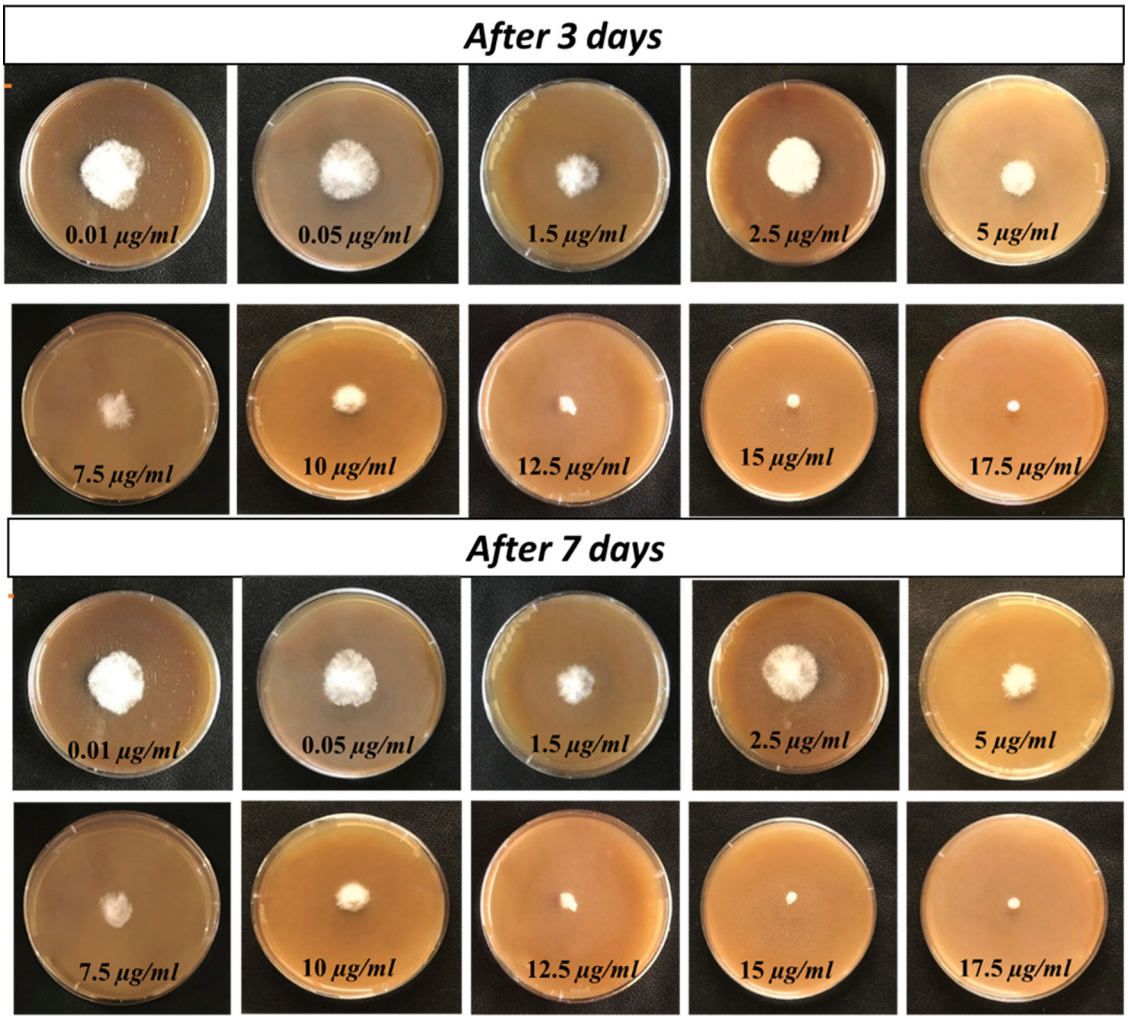

Fig. 9 Antifungal activity of iron oxide NPs at different concentrations (0.01–17.5 µg/ml) after three and seven days of incubation at 28 °C

inhibition of iron oxide NPs synthesized at pH (1–5, 7–9) are tabulated in Table S3. Inhibition zone tells that prepared NPs disturbed the cell wall, interfered with DNA (Deoxyribonucleic acid) transcription process and disrupted all chain reactions taking place in bacteria cell [57]. Reactive oxygen species (ROS) are accountable for oxidative stresses. ROS hold radicals of hydrogen peroxides (H_2O_2), super oxides (O_2^-) and radicals of hydroxide that can powerfully effect DNA structures and thiol groups of proteins present at bacterial surface. Increased zone of inhibition with reduced NPs size of 300 °C MFA sample at pH 6 [Fig. S1(a)] can be associated with the fact that smaller the size of NPs, greater would be the possibility to disturb the cell wall of bacteria [6]. Such NPs can induce oxidative stresses by reacting intracellular oxygen leading to cell membrane rupturing.

4.7 Photo catalytic activity

The treatment of water is one of the most serious problems globally due to the population growth and environmental issues. There are various technologies to tackle this problem. One of these technologies is photo catalytic degradation of organic compounds. Due to their visible light absorbance ability and low costs these are widely used nowadays [58]. Basically, photo catalytic activity is degradation of toxic organic compounds (i.e. methylene blue (MB)). Sunlight was used to irradiate the samples to evaluate the photo degradation capability of 300 °C MFA iron oxide NPs against MB under all pH levels. Photo catalytic activity, using test solutions, is done after every 15 min in total period of 1 h. The iron oxide NPs catalyzed degradation of MB under sunlight irradiation which is obvious from gradual decrease in characteristic absorption peak of MB with increase in time. It can be seen clearly (Fig. 8) that decrease in absorption peak of MB with time appeared and hence reached the base line showing effective degradation of dye due to NPs. Highest photo catalytic activity was obtained for magnetite NPs magnetically annealed at 300 °C synthesized at pH 6 and determined to be capable against dye of MB as shown in Fig. 8a.

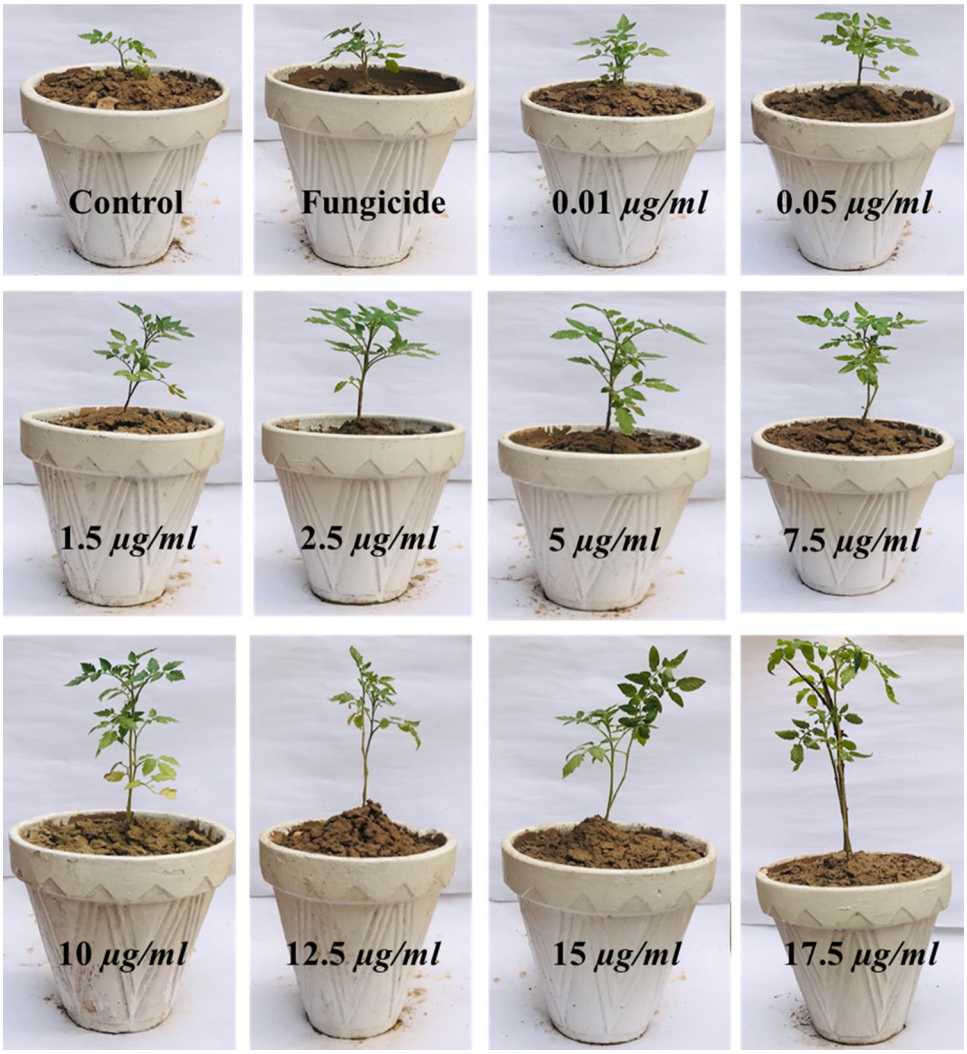

Fig. 10 Effect of concentrations of optimized iron oxide NPs on vegetative growth of tomato plant after 35 days under greenhouse effect infested with Fusarium oxysporum

Percentage of MB degradation using nanoparticles was calculated from Eq. 1.

Fig. 8b shows degradation (%) of dye using 300 °C MFA iron oxide NPs under all pH levels (1–9). It is observed that magnetite NPs at pH 6 exhibited maximum degradation of 92 % as compared to other iron oxide NPs. The NPs in the present study improved the formation of hydroxyl radical and helped in degradation of MB dye under sunlight irradiation. These findings can be correlated with XRD results (Fig. 2). The degradation process occurs on the surface of the catalyst. The electrons become excited on irradiation with light and then jump from valence band to empty conduction band. This results in electron-hole pair formation which are reducing as well as oxidizing agents. These excited electrons generate free radicals i.e. OH, O_2^- at surface of the catalyst on reacting with oxygen in reaction mixture [59, 60]. The whole process can also be seen in graphical abstract of the present work.

4.8 In-vitro antifungal efficiency

After initial screening, the iron oxide NPs at pH 6 MFA at 300°C were selected to be used for plant-based experiments. Magnetic nanoparticles are found to be potential candidate as a new generation fungicide due to antimicrobial and biocompatibility characteristics. Fig. 9 depicts the in-vitro effect of iron oxide NPs on Fusarium oxysporum at different concentrations (0.01 µg/ml −17.5 µg/ml). In cultured plates it showed suppressed fungal growth on 3rd and 7th day of incubation. It is observed that the least antifungal activity was observed at lowest concentrations both after 3rd and 7th day of incubation. Optimized iron oxide NPs at several concentrations prompted significant inhibition of fungus, depending on inoculum of fungus and concentrations of NPs. Large surface area to volume ratio of NPs is one of the responsible factors that can capably destroy the micro-organism by giving them less oxygen for

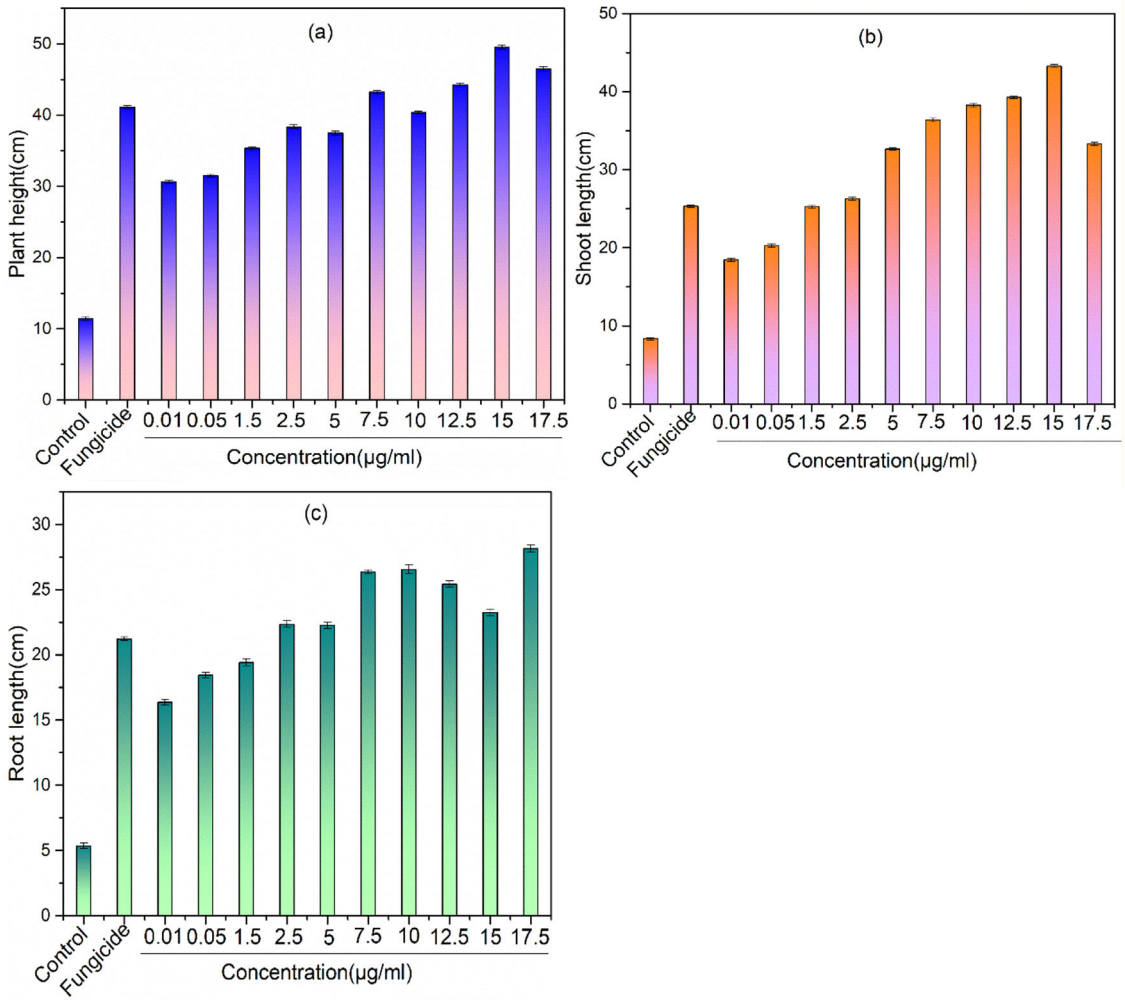

Fig. 11 Effect of concentrations of iron oxide NPs on plant height, root and shoot length infested with Fusarium wilt under greenhouse conditions. Vertical bars denote the standard deviation ($n = 3$) between the mean of different replicates of the same treatment using ANOVA and LSD tests at $P < 0.05$

respiration. Iron being powerful reducing agent, can affect the membrane proteins and lipo-polysaccharides by making the disintegration of functional groups. Fenton-reaction is responsible in iron oxide NPs for oxidation of intracellular-oxygen and eventually oxidative damage of cells by penetrating through dislocated membranes. Thus, it can be concluded that iron oxide NPs are capable to suppress the plant pathogenic fungi more powerfully as compared to other commercially available agrochemicals (i.e. fungicides and / or pesticides).

4.9 In-vivo efficacy of 300 °C MFA iron oxide nanoparticles (pH 6) on growth variables under greenhouse conditions

Optimized iron oxide nanoparticles were employed in pots under greenhouse conditions for their effectiveness against Fusarium oxysporum. Pots were filled with autoclaved sandy clay soil / loamy soil at 8 kg soil pot^{-1}. Spore suspension (50 ml) of fungus was inoculated in each pot and kept in a greenhouse for one week before sowing. Soil moisture was monitored on & off. Later, young seedlings were moved to the fungal treated pots. Next day, different concentrations of iron oxide NPs (0.01, 0.05, 1.5, 2.5, 5, 7.5, 10, 12.5, 15 and 17.5 µg/ml) were put in pots. When plant is enough established after transplanting then tomato plants were sprayed with two foliar sprays with an interval of ten days between each foliar spray. Different physiological parameters i.e. growth parameters were recorded after 35 days of growth. It can be observed that different concentrations of iron oxide NPs caused significant enhancement in growth parameters as compared to control and fungicide (Figs. 10–11). Growth parameters include plant height, shoot and root length, fresh and dry plant weight. Magnetic nanoparticles have capability to improve the growth parameters of tomato plant and have no bad effect,

so these NPs are capable to be used for higher productivity by decreasing disease [61]. Further, it was reported previously that iron oxide nanoparticles were used in peanut plant and increase in biomass and root length were observed [62]. According to the present study, application of iron oxide NPs at 17.5 µg/ml gave potential results for better growth parameters and inhibited the fungal infection entirely.

5 Conclusions

Sol-gel method was employed for synthesis of iron oxide NPs by varying pH values (1–9). Magnetic field annealing (MFA) of NPs was also done at different temperatures (200 and 300 °C). 300 °C MFA samples showed remarkable outcomes. XRD results showed magnetite phase (at pH 1, 2 & 6), mixed phases (at pH 3–5), maghemite phase (at pH 7-8) and hematite phase (at pH 9) for 300 °C MFA samples. SEM images showed particle size ~ 50 nm for 300 °C MFA iron oxide NPs (at pH 6). Raman spectroscopy results showed the formation of various phases of iron oxide NPs. Furthermore, 300 °C MFA magnetite nanoparticles (at pH 6) proved to be potential candidate against bacteria with inhibition zone ~ 31 mm and enhanced photo catalytic action (92 %) against MB dye. Magnetite NPs (pH 6) showed remarkable antifungal activity by inhibiting fungal growth both during in-vitro and in-vivo tests. According to the results, magnetite iron oxide can be suitable for biological control of both bacteria and fungus in protection of crops and degradation of dyes / organic pollutants.

Supplementary information The online version contains supplementary material available at https://doi.org/10.1007/s10971-023-06210-x.

Acknowledgements All authors are obliged to Higher Education Commission for financial support through grant no. HEC/CSSP/2020-2021. Authors are thankful to University of the Punjab for the financial support. The author extends appreciation to Researchers Supporting Project number (RSP2023R165), King Saud University, Riyadh, Saudi Arabia).

Author contributions Authors don't have known conflicting financial/ personal interactions that could have seemed to affect the present research.

Compliance with ethical standards

Conflict of interest The authors declare no competing interests.

References

1. Satheeshkumar MK, Kumar ER, Srinivas C, Suriyanarayanan N, Deepty M, Prajapat CL, Rao TC, Sastry DL (2019) Study of structural, morphological and magnetic properties of Ag substituted cobalt ferrite nanoparticles prepared by honey assisted combustion method and evaluation of their antibacterial activity. J Magn Magn Mat 469:691–697
2. Soares PI, Alves AM, Pereira LC, Coutinho JT, Ferreira IM, Novo CM, Borges JP (2014) Effects of surfactants on the magnetic properties of iron oxide colloids. J Colloid Interf Sci 419:46–51
3. Madubuonu N, Aisida SO, Ahmad I, Botha S, Zhao TK, Maaza M, Ezema FI (2020) Bio-inspired iron oxide nanoparticles using Psidium guajava aqueous extract for antibacterial activity. Appl Phys A 126(1):1–8
4. Nemati Z, Alonso J, Rodrigo I, Das R, Garaio E, García JÁ, Orue I, Phan MH, Srikanth H (2018) Improving the heating efficiency of iron oxide nanoparticles by tuning their shape and size. J Phys Chem C 122(4):2367–2381
5. Hashimoto H, Fujii T, Nakanishi M, Kusano Y, Ikeda Y, Takada J (2012) Synthesis and magnetic properties of magnetite-silicate nanocomposites derived from iron oxide of bacterial origin. Mater Chem Phys 136:1156–1161
6. Ismail RA, Sulaiman GM, Abdulrahman SA, Marzoog TR (2015) Antibacterial activity of magnetic iron oxide nanoparticles synthesized by laser ablation in liquid. Mater Sci Eng: C 53:286–297
7. Sangaiya P, Jayaprakash R (2018) Tuning effect of Sn doping on structural, morphological, optical, electrical and photocatalytic properties of iron oxide nanoparticles. Mater Sci Semicond Process 85:40–51
8. Gubin SP (Ed.) (2009) Magnetic nanoparticles. John Wiley & Sons
9. Bhowmik RN, Saravanan A (2010) Surface magnetism, Morin transition, and magnetic dynamics in antiferromagnetic α-Fe_2O_3 (hematite) nanograins. J Appl Phys 107:053916
10. Ramimoghadam D, Bagheri S, Hamid SBA (2014) Progress in electrochemical synthesis of magnetic iron oxide nanoparticles. J Magn Magn Mat 368:207–229
11. Olivera S, Hu C, Nagananda GS, Reddy N, Venkatesh K, Muralidhara HB, Asiri AM (2018) The adsorptive removal of Cr (VI) ions and antibacterial activity studies on hydrothermally synthesized iron oxide and zinc oxide nanocomposite. J Taiwan Inst Chem Eng 93:342–349
12. Ansari SAMK, Ficiarà E, Ruffinatti FA, Stura I, Argenziano M, Abollino O, Cavalli R, Guiot C, D'Agata F (2019) Magnetic iron oxide nanoparticles: synthesis, characterization and functionalization for biomedical applications in the central nervous system. Materials 12:465
13. Abhinayaa R, Jeevitha G, Mangalaraj D, Ponpandian N, Vidhya K, Angayarkanni J (2018) Cytotoxic consequences of Halloysite nanotube/iron oxide nanocomposite and iron oxide nanoparticles upon interaction with bacterial, non-cancerous and cancerous cells. Coll Surf B: Biointerf 169:395–403
14. Sarkar T, Tiwari S, Rawat K, Solanki PR, Bohidar HB (2017) Hydrophilic, fluorescent and superparamagnetic iron oxide-carbon composite nanoparticles. Colloids Surf A: Physicochem Eng Asp 514:218–225
15. Zare N, Zabardasti A, Mohammadi A, Azarbani F (2018) Synthesis of spherical Fe_3O_4 nanoparticles from the thermal decomposition of iron (III) nano-structure complex: DFT studies and evaluation of the biological activity. Bioorg Chem 80:334–346
16. Ashour AH, El-Batal AI, Maksoud MA, El-Sayyad GS, Labib S, Abdeltwab E, El-Okr MM (2018) Antimicrobial activity of metal-substituted cobalt ferrite nanoparticles synthesized by sol–gel technique. Particuology 40:141–151
17. Majumdar B, Sarma D, Jain S, Sarma TK (2018) One-pot magnetic iron oxide–carbon nanodot composite-catalyzed cyclooxidative aqueous tandem synthesis of quinazolinones in the

presence of tert-Butyl hydroperoxide. ACS Omega 3(10):13711–13719
18. Khedr MH, Halim KA, Soliman NK (2009) Synthesis and photocatalytic activity of nano-sized iron oxides. Mat Lett 63:598–601
19. Mohapatra M, Anand S (2010) Synthesis and applications of nano-structured iron oxides/hydroxides–a review. Int J Eng, Sci Technol 2:8
20. Romer S, Scheffold F, Schurtenberger P (2000) Sol-gel transition of concentrated colloidal suspensions. Phys Rev Lett 85(23):4980
21. Bustamante-Torres M, Romero-Fierro D, Estrella-Nuñez J, Arcentales-Vera B, Chichande-Proaño E, Bucio E (2022) Polymeric composite of magnetite iron oxide nanoparticles and their application in biomedicine: a review. Polymers 14(4):752
22. Kim SM, Chakrabarti K, Oh EO, Whang CM (2003) Effects of pH during the base catalyzed reaction of two-step acid/base catalyzed process on the microstructures and physical properties of poly (dimethylsiloxane) modified silica xerogels. J Sol-Gel Sci Technol 27:149–155
23. Kobayashi M, Sato Y, Sugimoto T (2022) Effect of pH and electrolyte concentration on sol–gel state of semi-dilute aqueous cellulose nanofiber suspension: an interpretation based on angle-dependent DLVO theory. Colloid Polym Sci 300(8):953–960
24. Imran M, Riaz S, Batool T, Qamar A, Khan IU, Zahoor R, Shahid A, Naseem S (2021) Biodistribution of iron-oxide-stabilized 99m Tc-ZrO 2 nanoparticles in rabbit using honey as a capping agent—microwave-assisted sol–gel approach. J Sol-Gel Sci Technol 98:95–112
25. Khan HN, Imran M, Sanaullah I, Khan IU, Sabri AN, Naseem S, Riaz S (2023) In Vivo biodistribution, antioxidant and hemolysis tendency of superparamagnetic iron oxide nanoparticles–potential anticancer agents. Arabian J Chem 16(4):104602
26. Matassini C, Parmeggiani C, Cardona F (2020) New frontiers on human safe insecticides and fungicides: An opinion on trehalase inhibitors. Molecules 25(13):3013
27. Vijayalakshmi K, Sivaraj D (2016) Synergistic antibacterial activity of barium doped TiO_2 nanoclusters synthesized by microwave processing. RSC Adv 6:9663–9671
28. Stauch C, Späth S, Ballweg T, Luxenhofer R, Mandel K (2017) Nanostructured micro-raspberries from superparamagnetic iron oxide nanoparticles: Studying agglomeration degree and redispersibility of nanoparticulate powders via magnetisation measurements. J Colloid Interf Sci 505:605–614
29. Ahn MS, Ahmad R, Bhat KS, Yoo JY, Mahmoudi T, Hahn YB (2018) Fabrication of a solution-gated transistor based on valinomycin modified iron oxide nanoparticles decorated zinc oxide nanorods for potassium detection. J Colloid Interf Sci 518:277–283
30. Wu W, He Q, Jiang C (2008) Magnetic iron oxide nanoparticles: synthesis and surface functionalization strategies. Nanoscale Res Lett 3(11):397–415
31. Passemard S, Staedler D, Učňová L, Schneiter GS, Kong P, Bonacina L, Gerber-Lemaire S (2013) Convenient synthesis of heterobifunctional poly (ethylene glycol) suitable for the functionalization of iron oxide nanoparticles for biomedical applications. Bioorg Med Chem Lett 23:5006–5010
32. Bloemen M, Brullot W, Luong TT, Geukens N, Gils A, Verbiest T (2012) Improved functionalization of oleic acid-coated iron oxide nanoparticles for biomedical applications. J Nanopart Res 14(9):1100
33. Gonzalez MB, Wu A, Vilarinho PM (2006) Influence of Solvents on the Microstructure and dielectric properties of $Ba_{0.5}Sr_{0.5}TiO_3$ thin films prepared by a diol-based sol− gel process. Chem Mater 18(7):1737–1744
34. Brown JS, Mohamed ZJ, Artim CM, Thornlow DN, Hassler JF, Rigoglioso VP, Alabi CA (2018) Antibacterial isoamphipathic oligomers highlight the importance of multimeric lipid aggregation for antibacterial potency. Commun Biol 1(1):220
35. Gruskiene R, Krivorotova T, Staneviciene R, Ratautas D, Serviene E, Sereikaite J (2018) Preparation and characterization of iron oxide magnetic nanoparticles functionalized by nisin. Coll Surf B: Biointerf 169:126–134
36. Samarakoon ERJ, Waduge R, Liu Q, Shahidi F, Banoub JH (2020) Impact of annealing on the hierarchical structure and physicochemical properties of waxy starches of different botanical origins. Food Chem 303:125344
37. Crippa F, Rodriguez-Lorenzo L, Hua X, Goris B, Bals S, Garitaonandia JS, Balog S, Burnand D, Hirt AM, Haeni L, Lattuada M, Rothen-Rutishauser B, Petri-Fink A (2019) Phase transformation of superparamagnetic iron oxide nanoparticles via thermal annealing: implications for hyperthermia applications. ACS Appl Nano Mater 2(7):4462–4470
38. Xu XN, Wolfus Y, Shaulov A, Yeshurun Y, Felner I, Nowik I, Gedanken A (2002) Annealing study of Fe_2O_3 nanoparticles: magnetic size effects and phase transformations. J Appl Phys 91(7):4611–4616
39. Du J, Li G, Liu S, Liu T, Wu C, Wang Q (2020) Enhancement of magnetic properties by adjusted structure in Fe nanocrystalline films via annealing and applying high magnetic field at different film-formation stages. J Magn Magnet Mater 495:165857
40. Prabhu Y, Rao KV, Kumari BS, Kumar VSS, Pavani T (2015) Synthesis of Fe_3O_4 nanoparticles and its antibacterial application. Int Nano Lett 5(2):85–92
41. Herrera A, Reyes A, Colina-Márquez J (2016) Evaluation of the photocatalytic activity of iron oxide nanoparticles functionalized with titanium dioxide. J Phys: Conf Series 687(1):012034. IOP Publishing
42. Chalangar, SE (2021) Synthesis and Characterization of ZnO/Graphene Nanostructures for Electronics and Photocatalysis (Vol. 2130). Linköping University Electronic Press, Colombia
43. Kumar M, Kumar V, Prasad R (Eds.) (2020) Phyto-microbiome in stress regulation. Springer, Berlin/Heidelberg, Germany
44. Xu J, Yang H, Fu W, Du K, Sui Y, Chen J, Zou G (2007) Preparation and magnetic properties of magnetite nanoparticles by sol–gel method. J Magn Magnet Mater 309(2):307–311
45. McHenry ME, Willard MA, Laughlin DE (1999) Amorphous and nanocrystalline materials for applications as soft magnets. Progr Mater Sci 44:291–433
46. Cullity BD (1956) Elements of X-ray diffraction. Addison-Wesley, Reading
47. Shah SMH, Riaz S, Hussain SS, Atiq S, Naseem S (2015) Structural, magnetic and dielectric properties of Ba doped $BiFeO_3$ thin films. Mater Today: Proc 2:5654–5659
48. Chithra MJ, Sathya M, Pushpanathan K (2015) Effect of pH on crystal size and photoluminescence property of ZnO nanoparticles prepared by chemical precipitation method. Acta Metallurgica Sinica (English Letters) 28(3):394–404
49. Kozakova Z, Kuritka I, Kazantseva NE, Babayan V, Pastorek M, Machovsky M, Bazant P, Sáha P (2015) The formation mechanism of iron oxide nanoparticles within the microwave-assisted solvothermal synthesis and its correlation with the structural and magnetic properties. Dalton Trans 44(48):21099–21108
50. Akbar A, Yousaf H, Riaz S, Naseem S (2019) Role of precursor to solvent ratio in tuning the magnetization of iron oxide thin films–A sol-gel approach. J Magn Magnet Mater 471:14–24
51. Upadhyay S, Parekh K, Pandey B (2016) Influence of crystallite size on the magnetic properties of Fe_3O_4 nanoparticles. J Alloys Comp 678:478–485
52. Radpour M, Alamolhoda S, Masoudpanah SM (2017) Effects of pH value on the microstructure and magnetic properties of solution combusted Fe_3O_4 powders. Cer Int 43(16):13729–13734

53. Khan S, Shah ZH, Riaz S, Ahmad N, Islam S, Raza MA, Naseem S (2020) Antimicrobial activity of citric acid functionalized iron oxide nanoparticles–Superparamagnetic effect. Cer Int 46(8):10942–10951
54. Lassoued A, Dkhil B, Gadri A, Ammar S (2017) Control of the shape and size of iron oxide (α-Fe_2O_3) nanoparticles synthesized through the chemical precipitation method. Res Phys 7:3007–3015
55. Singh, BP, Kumar, A, Areizaga-Martinez, HI, Vega-Olivencia, CA, & Tomar, MS (2017). Synthesis, characterization, and electrocatalytic ability of γ-Fe_2O_3 nanoparticles for sensing acetaminophen, 55(10), 722-728, NISCAIR-CSIR, India
56. Fox M (2002) Optical properties of solids. Oxford University Press, Oxford, UK, p 1269–1270
57. Lee C, Kim JY, Lee WI, Nelson KL, Yoon J, Sedlak DL (2008) Bactericidal effect of zero-valent iron nanoparticles on Escherichia coli. Environ Sci Technol 42(13):4927–4933
58. Saffari R, Shariatinia Z, Jourshabani M (2020) Synthesis and photocatalytic degradation activities of phosphorus containing ZnO microparticles under visible light irradiation for water treatment applications. Environ Pollut 259:113902
59. Baruah D, Yadav RNS, Yadav A, Das AM (2019) Alpinia nigra fruits mediated synthesis of silver nanoparticles and their antimicrobial and photocatalytic activities. J Photochem Photobiol B: Biol 201:111649
60. Olivo-Alanís D, Atilano-Camino MM, García-González A, Humberto-Álvarez L, García-Reyes RB (2021) Chlorophyll-sensitized phenolic resins for the photocatalytic degradation of methylene blue and synthetic blue wastewater. J Sol-Gel Sci Technol 100(3):538–554
61. Ashraf H, Batool T, Anjum T, Illyas A, Li G, Naseem S, Riaz S (2022) Antifungal potential of green synthesized magnetite nanoparticles black coffee–magnetite nanoparticles against wilt infection by ameliorating enzymatic activity and gene expression in solanum lycopersicum L. Front Microbiol 13:31
62. Rui M, Ma C, Hao Y, Guo J, Rui Y, Tang X, Zhu S (2016) Iron oxide nanoparticles as a potential iron fertilizer for peanut (Arachis hypogaea). Front Plant Sci 7:81